Orc6 dissociation from chromatin prevents premature loading of MCM at G2 and tetraploid production

Yoko Hayashi-Takanaka[1,2,*], Ichiro Hiratani[2], Tokuko Haraguchi[1] and Yasushi Hiraoka[1*]

[1] Graduate School of Frontier Biosciences, Osaka University, 1-3 Yamadaoka, Suita 565-0871, Japan

[2] RIKEN Center for Biosystems Dynamics Research, 2-2-3 Minatojima-minamimachi, Chuo-ku, Kobe 650-0047 Japan

[*]Correspondence should be addressed to:

Yoko Hayashi-Takanaka

RIKEN Center for Biosystems Dynamics Research, 2-2-3 Minatojima-minamimachi, Chuo-ku, Kobe 650-0047 Japan

E-mail: yoko.hayashi.yr@riken.jp

or

Yasushi Hiraoka

Graduate School of Frontier Biosciences, Osaka University, 1-3, Yamadaoka, Suita, 565-0871, Japan

E-mail: hiraoka@fbs.osaka-u.ac.jp

Abstract

DNA replication is tightly regulated to occur only once per cell cycle. The untimely initiation of DNA replication can result in genome instability, leading to aneuploidy, which has been associated with early senescence and cancer. The pre-replication complex, comprising the origin recognition complex (ORC; Orc1-6), Cdc6, Cdt1, and MCM, is required for initiating DNA replication, although the function of Orc6 is yet to be elucidated. Here, we show that Orc6 dissociates from chromatin upon entering the S-phase and that the Orc6 dissociation depends on proteasome activity. Treatment that inhibits proteasome activity, which declines with aging, increases the senescence marker p21 levels, and promotes cell cycle arrest in human immortalized hTERT-RPE1 cells. This treatment induced large nuclei with high levels of chromatin-bound Orc6 and MCM without undergoing mitosis. When the proteasome activity recovered, those cells with high levels of chromatin-bound Orc6 and MCM proceeded to whole-genome DNA replication, confirming that they were tetraploid G1 cells. We propose that proteasome-dependent dissociation of Orc6 from chromatin after S-phase is essential for preventing MCM reloading and the subsequent development of tetraploid cells.

Keywords

Aging/DNA replication/ORC/ pre-replication complex(pre-RC)/ tetraploid cells

Genomic DNA replication is essential for the proliferation of living organisms. In eukaryotes, this process is highly regulated to ensure that all chromosomes replicate once per cell cycle. An impairment of this process results in abnormal DNA replication, which can lead to genomic instability and promote senescence or oncogenesis (Thakur *et al*, 2022).

DNA replication begins with binding of pre-replication complexes (pre-RCs) to replication origins in the G1 phase (Hu & Stillman, 2023). The pre-RC comprises four types of proteins: the origin recognition complex (ORC), minichromosome maintenance (MCM), Cdc6, and Cdt1. MCM is a replicative helicase consisting of Mcm2–7 subunits (Bell & Botchan, 2013; Deegan & Diffley, 2016; Ishimi, 2018). Cdc6 and Cdt1 assist the recruitment of the MCM complex to chromatin. Upon entering the S-phase, the pre-RC disassembles. Abnormal pre-RC loading onto chromatin after the S-phase can initiate DNA re-replication before mitosis (Vassilev & DePamphilis, 2017; Limas & Cook, 2019). Therefore, after the onset of S-phase, Cdt1 and Cdc6 protein levels are highly regulated through proteasomal degradation mediated by E3 ubiquitin ligases (Nishitani *et al*, 2006; Walter *et al*, 2016).

ORC consists of the Orc1–6 hexamer and serves as a scaffold for assembling the other pre-RC components at the DNA replication origins during the G1 phase (Bell & Labib, 2016). In metazoans, replication origins do not share a distinct consensus sequence; instead, they are defined by their association with ORC binding. Metazoan ORC exists as a complete hexamer only during the G1 phase. Orc2–5 bind to chromatin throughout the cell cycle, whereas Orc1 selectively dissociates from chromatin via ubiquitin-mediated proteolysis after entering the S-phase (Li & DePamphilis, 2002; Méndez *et al*, 2002; Tatsumi *et al*, 2003). Orc1–5 exhibit structural similarities, whereas

Orc6 shows no structural similarity to other ORC subunits (Duncker *et al*, 2009), implying functional dissimilarity. Orc6 has the potential to independently bind to DNA regardless of Orc1-5 (Xu *et al*, 2020), participate in DNA repair (Lin *et al*, 2022), and contribute to mitosis (Bernal & Venkitaraman, 2011; Semple *et al*, 2006; Balasov *et al*, 2009) in various living organisms. However, the function of human Orc6 during the cell cycle remains largely unknown.

Proteasomes serve as the major cellular proteolytic machinery. Low levels of proteasome activity are observed in replicative senescent cells (Sabath *et al*, 2020), and its inhibition induces cellular senescence in normal human fibroblasts (Chondrogianni *et al*, 2003; Chondrogianni & Gonos, 2004; Ukekawa *et al*, 2004; Torres *et al*, 2006). Senescent cells are produced by evading mitosis and exhibit chromatin-bound pre-RCs, indicating their presence in the tetraploid G1 phase (Panopoulos *et al*, 2014; Johmura *et al*, 2014; Zeng *et al*, 2023). However, the role of proteasome activity in pre-RC formation during cellular senescence remains elusive.

In this study, we investigated changes in Orc6 levels during the cell cycle in human cells using multicolor immunofluorescence-based single-cell plot analysis (hereafter referred to as “single-cell plot analysis”). Single-cell plot analysis enables quantitative measurements of Orc6 levels in individual cells using fluorescence microscopy images (Hayashi-Takanaka *et al*, 2020, 2021). Therefore, it provides the advantage of not requiring cell synchronization when examining target protein levels during the cell cycle. In this study, we found that the continued presence of Orc6 on chromatin after the S phase entry resulted in the formation of tetraploid cells.

Results

Dissociation of Orc6 from chromatin during the S phase

To quantify chromatin-bound Orc6 in individual human cells, we performed single-cell plot analysis using fluorescence microscopy to measure multiple intracellular components within each cell (Hayashi-Takanaka *et al*, 2020, 2021). An asynchronous population of hTERT-RPE1cells was fixed using two different methods ("direct fixation" or "pre-extraction," Fig. 1A). The "direct fixation" method detects whole nuclear proteins, whereas the "pre-extraction" method only detects chromatin-bound fractions (Hayashi-Takanaka *et al*, 2021). The fixed cells were stained with Hoechst 33342 (DNA amount indicator, referred to as "Hoechst"), EdU (S-phase indicator), and an anti-Orc6 antibody (Fig. EV1). The same cells were stained with an anti-Orc2 antibody to detect the behavior of Orc2–5 subunits on chromatin throughout the cell cycle (Vashee *et al*, 2001; Dhar *et al*, 2001). The fluorescence images indicated that Orc6 staining was relatively uniform in the cell population prepared by the direct fixation method, whereas it was variable among the cells prepared by the pre-extraction method (compare the upper and lower panels for Orc6; Fig. 1A). In contrast, Orc2 staining was relatively uniform in both methods (right panels, Fig. 1A). Single-cell plot analysis was performed based on the images shown in Fig. 1A, and the normalized intensities of EdU, Orc6, and Orc2 were plotted against the DNA content determined by the Hoechst intensity (each dot represents one cell, Fig. 1B). EdU-positive S-phase cells (>-2 on the $\log_2$ scale) are denoted as orange dots in the EdU panels (left panels, Fig. 1B), and the same cells are denoted as orange dots in both Orc6 (middle panels, Fig. 1B) and Orc2 panels (right panels, Fig. 1B). In the direct fixation method, the whole fraction of Orc6 levels were relatively constant, ranging from -1 to 1 on the $\log_2$ scale throughout the cell cycle

(upper middle panel, Fig. 1B). In contrast, when employing the pre-extraction method, Orc6 levels in the chromatin-bound fraction were high in the G1 phase, decreased immediately after S-phase entry, and remained low in the S and G2 phases (lower middle panel, Fig. 1B). The Orc2 levels remained relatively constant at the G1/S transition and changed little during the S phase in both direct and pre-extraction methods (right panels, Fig. 1B). These results indicate that Orc6, but not Orc2, dissociates from chromatin during the S phase in hTERT-RPE1 cells.

To understand whether such Orc6 dissociation was also detected in other cell lines, we examined changes in chromatin-bound Orc6 levels during the cell cycle in cell lines derived from cancer cells (HeLa and U2OS cells) and normal fibroblast cells (IMR90 cells) using the pre-extraction method (Fig. EV2A, B). The decrease in Orc6 levels at the transition from G1 to S phase was smaller in cancer cell lines (HeLa and U2OS cells, Fig. EV2B) than in normal cell lines (IMR90 and hTERT-RPE1 cells, Fig. EV2B), suggesting that chromatin-bound Orc6 levels and their regulation during the cell cycle may vary between normal and cancer cells or between cell types.

Involvement of proteasome for dissociation of Orc6 from chromatin

As the levels of Cdt1, a component of the pre-RC, are regulated by proteasome activity, we investigated whether Orc6 was also a target for proteasome activity using MG132, a proteasome inhibitor. The hTERT-RPE1 cells were treated with 20 μM MG132 for varying durations (1, 2, and 4 h), fixed using the two different fixation methods, and stained with Hoechst and anti-Orc6 antibody. The same cells were co-stained with anti-Cdt1 and anti-Orc2 antibodies as controls for proteasomal degradation (Fig. 2A). Single-cell plot analysis showed that Orc6 levels in the whole fraction (obtained by the

direct-fixation method) remained almost unchanged for up to 2 h of MG132 treatment (blue dots, left panels in Fig. 2A), whereas those in the chromatin-bound fraction (obtained by the pre-extraction method) increased with MG132 treatment over time after the S phase (blue dots, right panels in Fig. 2A). Cdt1 levels (a positive control) increased in cells progressing through the S and G2 phases after 1 h of treatment and increased further with extended treatment periods in both fixation methods (orange dots, Fig. 2A), indicating that proteasomal degradation occurred normally in cells under these experimental conditions. Orc2 levels were almost unchanged for up to 4 h in the direct fixation method (green dots, left panels in Fig. 2A), and they slightly increased for 4 h treatment in the pre-extraction method (green dots, right panels in Fig. 2A). These results suggest that Orc6, and to a lesser extent Orc2, was not degraded by the proteasome during the S and G2 phases of the cell cycle but dissociated from chromatin via proteasome activity.

To compare the increase in Orc6 levels during the S phase due to MG132 treatment with that in Cdt1 and Orc2 levels, S-phase cells were selected based on the Hoechst value (1.1< Hoechst <1.75) from the single-cell plot analysis (Fig. 2A), and the fluorescence intensity of Orc6 in each cell was plotted against the Hoechst value (each dot represents a single cell, Fig. 2B). Plot analysis indicated that there were no or slight increases in the Orc6 and Orc2 levels in the whole fraction for up to 4 h treatment, whereas a large increase was observed in the total Cdt1 level with duration of MG132 treatment (whole fraction, Fig. 2B). Large increase was observed in the chromatin-bound fraction of Orc6 in S-phase cells with duration of MG132 treatment (Orc6, chromatin-bound fraction, Fig. 2B). The increase in chromatin-bound Cdt1 and Orc2 levels was lower than that in Orc6 (chromatin-bound fraction, Fig. 2B). Orc6

chromatin binding was not affected by depletion of Orc1 and Orc2 (Fig. EV3), suggesting that the increase in chromatin-bound Orc6 levels in MG132 treatment was not attributable to the presence of other ORC components on chromatin.

To further confirm this result, we examined Orc6 protein levels in whole-cell lysates and chromatin fractions obtained by sucrose cushion fractionation (Fig. 2C). Cells were treated with 20 μM MG132 for varying durations (1, 2, and 4 h), and Orc6 levels were analyzed in whole cell lysates and chromatin fractions using western blotting (Fig. 2D). The results indicated that the Orc6 levels in whole-cell lysates remained unchanged throughout MG132 treatment (whole, top row, Fig. 2D). In contrast, those in the chromatin fractions increased approximately 3-fold (top row, Fig. 2D). As a control, Cdt1 levels increased over time in the whole-cell lysates (approximately 7-fold) and chromatin fractions (approximately 3-fold) after MG132 treatment. Orc2 levels remained almost unchanged but slightly increased after the treatment (1.2–1.5-fold). These results are consistent with those of the single-plot analysis (Fig. 2A), suggesting that Orc6 dissociates from chromatin during the S phase via proteasome function without undergoing degradation.

Aged cells have high levels of chromatin-bound Orc6 after the S phase

To understand the relationship between Orc6 dissociation from chromatin and aging, we examined the dynamics of chromatin-bound Orc6 in human diploid fibroblast cells of different ages (Fig. 3A). IMR90 cells at passages 18 (younger cells) and 32 (older cells containing senescent cells) were fixed using the pre-extraction method and stained with Hoechst and anti-Orc6 antibody. The cells were co-stained with an anti-Mcm2 antibody as a marker for the cell cycle phases. Levels of chromatin-bound Mcm2 increase during

the G1 phase, peak at the G1/S transition, decrease during the S phase, and become lowest at the G2 phase (Mcm2, passage 18, Fig. 3B) (Zhou *et al*, 2020; Hayashi-Takanaka *et al*, 2021; Zeng *et al*, 2023). Immunostaining of passage 32 cells with an anti-Orc6 antibody occasionally showed enlarged nuclei with high levels of chromatin-bound Orc6 (arrows in Fig. 3A), whereas passage 18 cells did not (Fig. 3A). Single-cell plot analysis revealed the presence of cells with high Orc6 signals (Orc6 >0.5 on the $\log_2$ scale) and high DNA content (Hoechst >1.8) among passage 32 cells (magenta dots in the lower left panel, Fig. 3B). In contrast, a limited number of cells exhibiting these characteristics were observed among passage 18 cells (upper left panel in Fig. 3B). The cells with high Orc6 levels (magenta dots in the Orc6 panel) are plotted as magenta dots in the Mcm2 panel. Some of these magenta-marked cells (with high DNA content >1.8) showed low Mcm2 signals (blue-boxed region, Fig. 3B), indicating that these cells were in the G2 phase. These results suggest that Orc6 remained bound to chromatin until the G2 phase in a subset of aged cells. Additionally, some of the magenta-marked cells showed high Mcm2 signals (red-boxed region, Fig. 3B), suggesting that these cells were in a non-G2-phase state.

Induction of senescence by MG132 treatment causes aberrant loading of chromatin-bound Orc6 after the S phase

Senescent cells exhibit low proteasomal activity and impaired proteasome induces cellular senescence (Chondrogianni *et al*, 2003; Sabath *et al*, 2020). We first confirmed whether MG132 treatment induced cellular senescence in hTERT-RPE1 cells. We examined levels of p21 (a marker of cellular senescence) in cells treated with 312 nM MG132 for 18 h. Under these conditions, the incidence of cell death was lower than that

in treatment with higher concentrations (> 625 nM). Immunostaining using an anti-p21 antibody showed an increase in the number of the p21-positive cells by MG132 treatment compared with the DMSO control (Fig. 4A). Western blotting analysis also showed an increase in p21 protein levels by MG132 treatment compared with the DMSO control (Fig. 4B). These results suggest that inhibition of proteasome activity by MG132 induces the state similar to cellular senescence.

Next, we induced cellular senescence in immortalized hTERT-RPE1 cells by inhibiting proteasome activity with MG132 treatment and examined the Orc6 dynamics during the cell cycle. hTERT-RPE1 cells were treated with relatively low MG132 concentrations (78, 156, and 312 nM) for 18 h. Cells were fixed using the pre-extraction method, stained with anti-Orc6, anti-Mcm3, and anti-Cdt1 antibodies, and subjected to single-cell plot analysis (Fig. 4C). MG132 treatment produced cells with high levels of chromatin-bound Orc6 with high DNA content, which were denoted as magenta dots in Orc6 panels (Orc6 >0.5 on the $\log_2$ scale, Hoechst >1.8, Fig. 4C). The number of magenta cells increased with increasing MG132 concentrations. In contrast, few such cells appeared in the control DMSO cells (Fig. 4C). The cells labeled with magenta dots in Orc6 panels were also denoted as magenta dots in the Mcm3 and Ctd1 panels (middle and lower panels, Fig. 4C). Some of the magenta-marked cells had low Mcm3 signals (blue-boxed region, Fig. 4C; blue arrows, Fig. EV4A), indicating that these cells were in the G2 phase. Notably, other magenta-marked cells had high Mcm3 levels (red-boxed region, Fig. 4C; red arrows, Fig. EV4A), suggesting that these cells are in a non-G2-phase state. Co-staining with Cdt1 showed that most of the magenta-marked cells exhibited relatively high levels of Cdt1 compared with those of G2 phase cells in

the DMSO control. Based on these observations, we hypothesized that these red-boxed cells with high Mcm3 levels represent G1-phase cells.

Defects in the proteasome cause the formation of tetraploid cells

To elucidate the emergence of high-Orc6 cells with high DNA content (magenta dots in Fig. 4C) by MG132 treatment, we performed a time-course analysis of MG132 treatment (Fig. 4D) and analyzed cell cycle stages of the cells by staining with anti-Mcm2 (G1-phase marker) and anti-histone H3 phosphorylated at the 10th serine residue (H3S10ph; M-phase marker) antibodies (Hayashi-Takanaka *et al*, 2009). When cells were treated with DMSO as a control, cells with high histone H3S10ph signals were detected (magenta dots, Fig. 4D; Fig. EV4B), indicating normal cell cycle progression under these conditions (leftmost, lower panel, Fig. 4D). In contrast, upon treatment with MG132, cells with high histone H3S10ph signals gradually disappeared by 8 h. The number of cells with high DNA content (Hoechst ~2) and low Mcm2 levels gradually increased for 4–12 h (blue-circled regions, Fig. 4D), suggesting that the first 4–12 h of treatment resulted in the accumulation of G2-phase cells. Longer MG132 treatments (16–24 h) showed an increase in the number of cells with high DNA content (Hoechst ~2) and high Mcm2 levels (red-boxed regions, Fig. 4D). During the 16–24 h period, no M-phase cells were observed. These results suggest that the cells with high DNA content (Hoechst, ~2) and high Mcm2 levels represent tetraploid G1 cells produced by skipping the M phase. We also confirmed that 24 h treatment with MG132 produced large nuclei with high levels of cyclin B1 (Fig. EV4C), which is expressed in the late G2 and mitosis phases but less in the G1 phase (Behbehani *et al*, 2012). This

result suggests that the aberrant loading of MCM onto chromatin begins in the G2 phase.

To clarify the involvement of proteasomes in the formation of tetraploid G1 cells, we examined the depletion effects of PSMD7, a 26S proteasome subunit, required for proteolytic activity (Shi *et al*, 2018), using siRNA treatment. Cells were subjected to a 2-day treatment with siRNA targeting PSMD7. Western blotting analysis showed that the amount of PSMD7 was reduced to approximately 20% of that of the control siRNA (Fig. 4E). Under these conditions, siRNA-treated cells were fixed using the pre-extraction method, stained with anti-Orc6 and anti-Mcm2 antibodies, and subjected to single-cell plot analysis (Fig. 4F). The results showed that PSMD7 depletion produced cells with high chromatin-bound Orc6 levels and high DNA content (magenta dots, Orc6 >0.5 on the $\log_2$ scale, Hoechst >1.8, Fig. 4F). Some of these cells exhibited low Mcm2 levels signifying the G2 phase (blue-boxed region, Fig. 4F), whereas others exhibited high Mcm2 levels signifying the G1 phase (red-boxed region, Fig. 4F), suggesting that PSMD7 plays a role in dissociation of Orc6 from chromatin at the onset of S phase. These results also suggest that proteasome defects are responsible for the abnormal loading of Orc6 onto chromatin after the S phase, leading to the production of tetraploid G1 cells.

Tetraploid cells formed by proteasome inhibition progress to the S phase

We hypothesized that cells with abnormal MCM loading onto chromatin, with a Hoechst value of approximately 2, would undergo DNA replication without mitosis. To investigate this hypothesis, cells were treated with 312 nM MG132 for 24 h (day 1), washed, and cultured in a fresh MG132-free medium for 24 h (day 2), and DNA

synthesis was monitored (Fig. 5A). To label cells undergoing DNA replication, EdU was added to the culture medium 30 min prior to fixation at the end of day 1 or 2. Subsequently, the cells were fixed using the pre-extraction method, stained with EdU, anti-Mcm2, and anti-Orc6 antibodies, and subjected to single-cell plot analysis (Fig. 5B). EdU-positive cells were denoted as orange dots, and the same cells were also denoted as orange dots in the Mcm2 and Orc6 panels (Fig. 5B). The results showed that on day 1 of cell culture with MG132, the number of EdU-positive cells was limited, with the majority of the cells being arrested at Hoechst levels of 1 or 2. Among the cells with Hoechst levels of approximately 2, some cells had high levels of Mcm2 (red-boxed regions, Fig. 5B). One day after MG132 removal (day 2), EdU-positive cells were detected with Hoechst ranges of 1–2 and 2–4 (orange dots, day-2 panels, Fig. 5B). These results indicate that cells with Hoechst levels of 2–4 were produced by an additional round of DNA replication, implying the occurrence of whole-genome duplication in these cells (EdU panels, day 2, Fig. 5B). Mcm2 patterns exhibited similarities between cell populations with Hoechst levels 1–2 and 2–4 (Mcm2 panel, day 2, Fig. 5B): Mcm2 levels increased during the G1 phase and decreased during the S phase, reaching their lowest levels in the G2 phase. These results suggest that cells with high Mcm2 levels and DNA content of Hoechst ~2 (red-boxed region, Fig. 5B) proceeded to another round of DNA replication.

To understand the cell cycle phases of cells with high Orc6 levels and DNA content of Hoechst ~2, these cells were denoted as magenta dots in the Orc6 panels (Orc6 > 0.5 on the $\log_2$ scale, Fig. 5B'). The same cells were denoted as magenta dots also in the Mcm2 panels (Fig. 5B'). As indicated in Fig. 4C, high Orc6 cell populations with DNA content of Hoechst ~2 were divided into two groups on day 1: one group

exhibited high Mcm2 levels, whereas the other exhibited relatively low Mcm2 levels (red- and blue-boxed regions, respectively, Fig. 5B'; red and blue arrows, respectively, Fig.5C). In contrast, most of the high Orc6 cell population exhibited high Mcm2 levels on day 2, indicating that these cells were in the G1 phase. These results suggest that some of the high-Orc6 cells with DNA content of Hoechst ~2 are tetraploid G1 cells, whereas others are diploid G2 cells. These results also suggest that tetraploid cells produced by proteasome inhibitors can undergo DNA replication.

Involvement of Orc6 in MCM loading during tetraploid formation

To investigate whether the presence of Orc6 on chromatin after S phase entry contributes to MCM loading, we performed proteasome inhibitor treatment following siRNA treatment to deplete the Orc6 protein. Initially, cells were treated with Orc6 siRNA (siOrc6) for 42 h to assess the effect of Orc6 depletion alone on MCM loading (Fig. 6A). Western blotting analysis confirmed that siRNA targeting Orc6 efficiently reduced the total amount of Orc6 protein (Fig. 6B), and the chromatin-bound Orc6 (Fig. EV3B). Following a 42-h siRNA treatment, the cells were fixed using the pre-extraction method and stained with Hoechst and anti-Mcm2 antibody. Single-cell plot analysis showed that the distribution pattern of siOrc6-treated cells resembled that of the negative control (Fig. 6C, Fig. EV5A). As a positive control, we examined the effect of Orc1 depletion, as Orc1 is a subunit essential for MCM loading on chromatin (Ogawa *et al*, 1999; Samson *et al*, 2016; Coulombe *et al*, 2019) and is degraded in a proteasome-dependent manner after the S-phase entry (Li & DePamphilis, 2002; Méndez *et al*, 2002; Tatsumi *et al*, 2003). Upon treatment with Orc1 siRNA (siOrc1), chromatin-bound Mcm2 levels were reduced compared to that in the negative control

(Fig. 6C), and the number of G1-phase cells increased while the number of S-phase cells decreased (Fig. EV5A). These results confirmed the significance of Orc1 for Mcm2 loading onto chromatin during the S phase and indicated that Orc1 depletion moderately arrested the cell cycle at the G1 phase in hTERT-RPE1 cells. In contrast, Orc6 depletion with siRNA had a weaker effect on Mcm2 loading onto chromatin when compared to that in Orc1 (Fig. 6C and Fig. EV5A).

Next, we examined the effect of Orc6 depletion on the loading of Mcm2 onto chromatin induced by proteasome-inhibitor treatment. Cells were treated with siRNA for 18 h, followed by MG132 treatment for an additional 24 h under siRNA treatment (Fig. 6D, Fig. EV5B). Following the treatment, cells were fixed using the pre-extraction method, stained with Hoechst and anti-Mcm2 antibody, and then analyzed using single-cell plot analysis. The results showed that cells with high Mcm2 levels and DNA content of Hoechst ~2, that is, cells with MCM loading on chromatin after the S phase, were observed in the negative control (siControl, Fig. 6E). These cells were recognized as tetraploid G1 cells formed by skipping the M phase due to proteasome-inhibitor treatment, as mentioned above (Fig. 4E). These tetraploid G1 cells with high MCM levels (Hoechst >1.8 and Mcm2 >−2 on the $\log_2$ scale) were selected (magenta dots, Fig. 6E) and quantified as a percentage of the total number of cells with Hoechst signals >1.8 (Fig. 6F). The results showed that the percentage of tetraploid cells with high MCM levels was 35.2 ± 6.7% in the siControl. In contrast, in Orc1-depleted cells, it was significantly reduced to 5.7 ± 2.4% (Fig. 6F), indicating the significance of Orc1 in MCM loading in tetraploid G1 cells. Similarly, the percentage of high-MCM cells was reduced to 13.3 ± 8.4% in Orc6-depleted cells compared to that in the siControl (p =

0.0006, Fig. 6F). These results suggest that Orc6 is involved in the reloading of MCM in tetraploid G1 cells, albeit to a lesser extent than Orc1.

We also examined the involvement of Cdc6, another pre-RC component, in MCM loading following siRNA treatment. Western blotting analysis confirmed the effective reduction of Cdc6 protein levels using siRNA (Fig. 6G). Cells were treated with siRNA targeting Cdc6 for 18 h and then treated with MG132 for an additional 24 h (Fig. 6D). The cells were fixed using the pre-extraction method and stained with Hoechst and anti-Mcm2 antibody. Single-cell plot analysis showed a reduction in the number of tetraploid G1 cells exhibiting high MCM levels (magenta dots, Hoechst >1.8, and Mcm2 >−2 on the $\log_2$ scale) upon depletion of Cdc6 siRNA (Fig. 6H), similar to Orc6 siRNA effects. Therefore, Orc6 and another pre-RC factor, Cdc6, are involved in the chromatin loading of MCM during the tetraploid G1 phase.

In summary, during the G1 phase, Orc6 binds to chromatin in conjunction with other pre-RC components. Upon entering the S phase, Cdt1 and Orc1 proteins are degraded by proteasome activity, while Orc6 is dissociated from the chromatin (Fig. 7A). Orc2–5 remain on chromatin throughout the cell cycle. These cells progress to mitosis, producing normal diploid cells (Fig. 7A). When cells lose proteasome activity, Orc6, Orc1, Cdt1, and MCMs are prematurely reloaded onto chromatin without progressing to mitosis, thereby producing tetraploid cells (Fig. 7B).

Discussion

In this study, we demonstrated the dynamic changes in chromatin-bound Orc6 levels during the cell cycle in hTERT-RPE1 cells. The chromatin-bound Orc6 levels increased until the G1/S transition, decreased upon entering the S phase, and remained low until

the next G1 phase, although the total amount of Orc6 was almost unchanged during the cell cycle. Contradictory to our results, previous western blotting analysis using synchronized HeLa cells in different cell cycle phases showed that the levels of chromatin-bound Orc6 were nearly constant throughout the cell cycle (Méndez *et al*, 2002). Our single-cell plot analysis showed that the difference in the Orc6 levels between the G1 and S/G2 phases in two cancer cell lines (HeLa and U2OS cells) was smaller than that in normal cell lines (IMR90, and hTERT-RPE1 cells) (Fig. 1, Fig. EV2). This suggests that regulating chromatin-bound Orc6 levels during the cell cycle could potentially serve as a distinguishing factor between cancer and normal cells.

We demonstrated that Orc6 removal from chromatin after the S phase by a proteasome-dependent mechanism plays a significant role in inhibiting abnormal MCM loading. Aberrant MCM loading onto chromatin after the S phase can induce an additional round of DNA replication without mitotic division, leading to tetraploidy and consequent cancer development. To prevent this, the ubiquitin-proteasome system regulates the protein levels of pre-RC factors such as Cdt1, Cdc6, and Orc1 during the cell cycle (Nishitani *et al*, 2006; Walter *et al*, 2016; Li & DePamphilis, 2002; Méndez *et al*, 2002; Tatsumi *et al*, 2003). Orc6 is not degraded at the protein level and is dissociated from chromatin by proteasome activity. Therefore, proteasome activity is presumed to differently regulate pre-RC protein levels on chromatin, thereby preventing abnormal MCM loading. Given that Orc6 is the most diverse ORC subunit protein (Dhar & Dutta, 2000), its dissociation from chromatin during the S phase may have evolved as a new mechanism to prevent aberrant MCM loading onto chromatin.

The molecular mechanism underlying Orc6 dissociation from chromatin remains uncertain. Orc6 has no known ubiquitinated amino acid residues for subsequent

proteasomal degradation (Coulombe *et al*, 2019). A possible explanation is the involvement of post-translational modifications, such as phosphorylation, as observed in S. cerevisiae Orc6 (Chen *et al*, 2007; Chen & Bell, 2011). Recently, the significance of S-phase-specific Orc6 phosphorylation for genome stability through DNA damage checkpoints has been reported (Lin *et al*, 2023). These protein modifications could be responsible for Orc6 dissociation from chromatin, mediated by proteasome activity through the degradation of modifying enzymes. Moreover, proteasomes may have nonproteolytic functions. Multiple ATPases within the proteasome enable DNA unwinding (Makino *et al*, 1996, 1999). Consequently, a proteasome lacking proteolytic activity can facilitate DNA unwinding, allowing chromatin binding to ORC, including Orc6. Furthermore, proteasome activity inhibition can induce nucleosome hyperacetylation at transcription start sites (Kinyamu *et al*, 2020), which coincides with replication origins (Sugimoto *et al*, 2018), potentially facilitating the chromatin binding of Orc6.

Reduced proteasome activity impairs various cellular activities, including senescence (Vilchez *et al*, 2014; Huang *et al*, 2022). Recent studies have shown that cellular senescence corresponds to a tetraploid state in the G1 phase, which appears when cells skip the M phase (Panopoulos *et al*, 2014; Johmura *et al*, 2014; Zeng *et al*, 2023). Consistently, we observed that inhibition of proteasome activity by MG132 resulted in tetraploid G1 cells, and that subsequent removal of the inhibitor restored proteasome activity, promoting cell progression to the S phase (Figs. 4, 5). Therefore, reduction in proteasome activity during aging may result in the production of tetraploid G1 cells, thereby increasing the risk of cancer development.

Our results indicate the involvement of pre-RC factors Orc6, Orc1, and Cdc6 in tetraploid cell production. Although the deletion of either Orc1 or Orc2 has a profound effect on cell cycle progression (Okano-Uchida *et al*, 2018; Chou *et al*, 2021), Orc6 siRNA had a minimal effect on cell cycle progression in hTERT-RPE1 (Fig. 6, this study) and U2OS cells (Lin *et al*, 2022). These results suggest that incomplete ORC hexamers could recruit pre-RC to chromatin after the S phase in differentiated cells, although all subunits of the Orc1–6 hexamer are presumably essential in undifferentiated cells such as those in early embryogenesis (Prasanth *et al*, 2002; Ortega *et al*, 2016). Therefore, it may be important to eliminate both Orc1 and Orc6 from the chromatin at the onset of the S phase. Certain carcinomas with elevated Orc6 levels (Pan *et al*, 2022; Tang *et al*, 2023) indicate that the presence of excessive amounts of Orc6 might hinder Orc6 dissociation from chromatin, potentially resulting in the reloading of pre-RC onto chromatin. Our findings indicate that normal cells can progress to the tetraploid G1 phase when the proteasome activity is reduced, a significant step associated with whole-genome duplication related to carcinogenesis (Bielski *et al*, 2018; López *et al*, 2020; Gemble *et al*, 2022). Therefore, our findings advance comprehension of the emerging replication factor dynamics through proteasome activity and correlate with the process of tetraploid cell formation, which is associated with senescence and cancer development.

Materials and Methods

Antibodies for immunostaining

The primary antibodies used were anti-Orc6 (3A4, sc-32735; Santa Cruz Biotechnology), anti-Orc2 (M055-3, MBL), anti-Cdt1 (D10F11; Cell Signaling

Technology), anti-Mcm3 (sc-390480; Lot#J1118, Santa Cruz Biotechnology; Anti-BM28; 610700, BD transduction), anti-Mcm2 (D7G11, Cell Signaling Technology), anti-Orc1 (F-10, sc-398734, Santa Cruz Biotechnology), anti-GAPDH (14C10; Cell Signaling Technology), anti-histone H3 (1G1) (Nozawa *et al*, 2010), anti-PSMD7 (EPR13517, ab181072; Abcam), anti-Cdc6 (sc-9964, Santa Cruz Biotechnology), anti-p21 (12D1; Cell Signaling Technology), anti-histone H3S10ph (CMA311, (Hayashi-Takanaka *et al*, 2009)) and cyclin B1 (AB_397617, BD biosciences). The specificity of these antibodies used for immunostaining is shown in Fig. EV1. We previously confirmed by single-cell plot analysis based on immunostaining that chromatin-bound Mcm2 and Mcm3 showed similar dynamics during the cell cycle (Hayashi-Takanaka *et al*, 2021).

For fluorescent staining, the secondary antibodies were as follows: Alexa 488 donkey anti-mouse IgG (715-545-151; Jackson ImmunoResearch), Cy5 donkey anti-mouse IgG (715-175-151; Jackson ImmunoResearch), Cy3 donkey anti-Rat IgG (712-165-153; Jackson ImmunoResearch), Alexa 488 donkey anti-rabbit IgG (711-545-152; Jackson ImmunoResearch) and Cy3 donkey anti-rabbit IgG (711-005-152; Jackson ImmunoResearch).

Cell culture and chemicals

hTERT-RPE1 (ATCC, CRL-4000), IMR90 (ATCC, CCL-186), U2OS (ATCC, HTB-96), and HeLa (RCB0007) cell lines were grown in a culture medium containing high-glucose Dulbecco’s modified Eagle’s medium (Sigma-Aldrich) supplemented with penicillin/streptomycin (100 units/mL penicillin, 100 μg/mL streptomycin; Fujifilm) and 10% fetal calf serum (Thermo Fisher Scientific), as previously described

(Hayashi-Takanaka *et al*, 2021).

siRNA transfection was performed using Lipofectamine RNAiMAX (Thermo Fisher Scientific) with siRNAs (SASI_Hs01_00069342 for Orc6, SASI_Hs01_00038888 for Orc1, SASI_Hs02_00341067 for Orc2, and Universal Negative Control #1, Sigma-Aldrich; s11403 for PSMD7, and s2745 for Cdc6, Ambion, Thermo Fisher Scientific) in accordance with the manufacturer's protocol.

MG132 (Fujifilm) was dissolved in DMSO.

Fluorescence staining for single-cell plot analysis

Immunostaining was performed as previously described (Hayashi-Takanaka *et al*, 2011, 2021, 2015). Briefly, the cells (~2×10^4 cells/cm^2) were plated on a 12-well plate with a coverslip (15 mm diameter; No. 1S; Matsunami) at the bottom and cultured for more than 1 day.

In the direct fixation method, cells were first fixed with 1 mL of the fixative (2% paraformaldehyde [Electron Microscopy Sciences] dissolved in 250 mM HEPES [pH 7.4]) for 10 min at room temperature (approximately 25°C), followed by permeabilization for 15 min using 1 % Triton X-100 in PBS, and subsequently blocked with Blocking One (Nacalai Tesque, Inc.).

In the pre-extraction method, prior to fixation, cells were first treated with 1 mL of 0.2% Triton X-100 solution containing 20 mM HEPES (pH 7.4), 100 mM NaCl, and 300 mM sucrose for 3 min on ice. After removing the Triton X-100 solution, the cells were then fixed using the fixative described above. This fixation method removes the nuclear membranes and loosely bound chromatin proteins.

The fixed cells were incubated with specific primary antibodies (0.2–1 μg/mL)

for 2 h at room temperature (approximately 25°C) and washed three times (10 min each) using PBS. When cells were stained with multiple antibodies, the cells were simultaneously incubated with these antibodies. The cells were treated with secondary antibodies (1 μg/mL) and Hoechst (0.1 μg/mL) for 2 h at room temperature (approximately 25°C) and subsequently washed three times with PBS. The cells were mounted using the ProLong Glass Antifade Mountant (Thermo Fisher Scientific).

The replication foci were labeled by culturing the cells in a medium containing 10 μM 5-ethynyl-2′-deoxyuridine (EdU) for 30 min. Subsequently, the cells were fixed using the direct fixation or pre-extraction method, and the resulting EdU signals were detected with Alexa Fluor 647 using a Click-iT EdU Imaging Kit (Thermo Fisher Scientific).

Microscopy

Fluorescence images were obtained using a DeltaVision Elite system (GE Healthcare Inc.) equipped with a pco.edge 4.2 sCMOS camera (PCO) and an Olympus 40× UApo/340 oil immersion objective lens (NA 0.65 with iris) with DeltaVision Elite Filter Sets (DAPI-FITC-TRITC-Cy5).

Single-cell plot analysis

Single-cell plot analysis was used to measure the levels of multiple intracellular components based on fluorescence microscopic images and plot their correlation in individual cells (Hayashi-Takanaka *et al*, 2020, 2021). The fluorescence intensity of each nucleus was measured using NIS Elements software (version 3.0; Nikon). The background intensity outside the cells was subtracted. The nuclear areas of individual

cells were determined by automatic thresholding using Hoechst signals. The sum of the intensities (i.e., the average intensity × nuclear area) in each nucleus was measured across all the fluorescence channels. Cells in the M phase were excluded from analysis, except for those shown in Fig. 4D. In Fig. 4D, M-phase cells were used for the analysis. To plot the Hoechst intensity distribution of 450–600 nuclei, the signal intensity in each nucleus was normalized relative to those with the 20th lowest and 20th highest intensities, designated as 1 and 2, respectively, because nuclei with the lowest and highest intensities were sometimes outliers. Hoechst intensity was plotted on a linear scale. The average intensities of Orc6, EdU, Orc2, Cdt1, Mcm2, and Mcm3 were set to 1 (0 on the $\log_2$ scale) and plotted on the $\log_2$ scale. The fluorescence intensities were normalized to time "0 h" (Figs. 2A, 2B), DMSO treatment (Figs. 4D, 4E, EV4C, EV4D), the negative control siRNA (Figs. 6C, 6E, 6H, EV3A, EV4F, EV4D) and MG132 treatment for day 1 (Fig. 5). The values relative to the average were plotted using Mathematica (version 13.0) (Wolfram Research).

Preparation of chromatin fractions and whole-cell lysates

Native chromatin fractions (hereafter, referred to as "chromatin fractions") were prepared by the method previously described (Sheu & Stillman, 2006; Quan *et al*, 2015) with some modifications (Hayashi-Takanaka *et al*, 2021). The cells were washed with cold PBS, suspended in buffer A (50 mM HEPES [pH 7.4], 100 mM KCl, 2.5 mM $MgCl_2$, 0.1 mM $ZnSO_4$, 1 mM ATP, 1 mM dithiothreitol [DTT], and protease inhibitor cocktail [EDTA-free, Nacalai Tesque, Inc.]), and collected via centrifugation (1,300 *g*, 3 min, 4°C). The cells were subsequently treated with 200 µL of 0.2% Triton X-100 in buffer A, layered with 200 µL of 30% sucrose cushion in buffer A containing 0.2%

Triton X-100, and centrifuged at 20,000 × *g* for 10 min at 4°C. The pellets were collected as chromatin fractions and dissolved in 1× SDS loading buffer. The suspension was then subjected to SDS-PAGE.

To prepare whole-cell lysates, the cells were washed with PBS and suspended in an equal volume of 2× SDS loading buffer. The suspension was subjected to SDS-PAGE.

Western blotting analysis

Chromatin fractions and whole-cell lysates were suspended in 1× SDS loading buffer and subjected to 10%, 12% or 15% SDS-PAGE to separate proteins. Proteins were transferred onto Immobilon-P PVDF membranes (Merck) using a semi-dry blotting system (ATTO). After blocking with 5% skim milk (Nacalai Tesque, Inc.), the membranes were incubated with the primary antibodies. After incubation with peroxidase-conjugated secondary antibodies (GE Healthcare), the signals were detected using ImmunoStar LD (Fujifilm Wako).

Acknowledgements

We thank Ms. Chizuru Ohtsuki and Yoshino Kubota for their technical assistance, and Drs. Hisao Masai, Haruhiko Asakawa, and Yasuhiro Hirano for insightful discussion. We also thank Dr. Hiroshi Kimura for histone H3 antibodies and Dr. Hisao Masukata for critically reading the manuscript.

This work was supported by JSPS KAKENHI grants: JP18H05530, JP20K20582 and JP20K08698 (to IH); JP18H05533, JP20H00454 and JP23K05636 (to YH); and JP18H05528 (to TH). This work was also supported by the Naito Foundation,

Urakami Foundation for Food and Food Culture Promotion, and the Foundation for Promotion of Cancer Research in Japan (to YHT).

Data Availability

Source data are available from the corresponding authors upon reasonable request.

Conflict of interest

The authors declare no competing interests.

References

Balasov M, Huijbregts RPH & Chesnokov I (2009) Functional analysis of an Orc6 mutant in Drosophila. *Proc Natl Acad Sci U S A* 106: 10672–10677

Behbehani GK, Bendall SC, Clutter MR, Fantl WJ & Nolan GP (2012) Single-cell mass cytometry adapted to measurements of the cell cycle. *Cytometry A* 81: 552–566

Bell SD & Botchan MR (2013) The minichromosome maintenance replicative helicase. *Cold Spring Harb Perspect Biol* 5: a012807

Bell SP & Labib K (2016) Chromosome Duplication in Saccharomyces cerevisiae. *Genetics* 203: 1027–1067

Bernal JA & Venkitaraman AR (2011) A vertebrate N-end rule degron reveals that Orc6 is required in mitosis for daughter cell abscission. *J Cell Biol* 192: 969–978

Bielski CM, Zehir A, Penson AV, Donoghue MTA, Chatila W, Armenia J, Chang MT, Schram AM, Jonsson P, Bandlamudi C, *et al* (2018) Genome doubling shapes the evolution and prognosis of advanced cancers. *Nat Genet* 50: 1189–1195

Chen S & Bell SP (2011) CDK prevents Mcm2–7 helicase loading by inhibiting Cdt1 interaction with Orc6. *Genes Dev* 25: 363–372

Chen S, De Vries MA & Bell SP (2007) Orc6 is required for dynamic recruitment of Cdt1 during repeated Mcm2–7 loading. *Genes Dev* 21: 2897–2907

Chondrogianni N & Gonos ES (2004) Proteasome inhibition induces a senescence-like phenotype in primary human fibroblasts cultures. *Biogerontology* 5: 55–61

Chondrogianni N, Stratford FLL, Trougakos IP, Friguet B, Rivett AJ & Gonos ES (2003) Central role of the proteasome in senescence and survival of human fibroblasts: induction of a senescence-like phenotype upon its inhibition and resistance to stress upon its activation. *J Biol Chem* 278: 28026–28037

Chou H-C, Bhalla K, Demerdesh OE, Klingbeil O, Hanington K, Aganezov S, Andrews P, Alsudani H, Chang K, Vakoc CR, *et al* (2021) The human origin recognition complex is essential for pre-RC assembly, mitosis, and maintenance of nuclear structure. *Elife* 10: e61797

604 Coulombe P, Nassar J, Peiffer I, Stanojcic S, Sterkers Y, Delamarre A, Bocquet S &
605 Méchali M (2019) The ORC ubiquitin ligase OBI1 promotes DNA replication
606 origin firing. *Nat Commun* 10: 2426

607 Deegan TD & Diffley JF (2016) MCM: one ring to rule them all. *Current Opinion in*
608 *Structural Biology* 37: 145–151

609 Dhar SK, Delmolino L & Dutta A (2001) Architecture of the human origin recognition
610 complex. *J Biol Chem* 276: 29067–29071

611 Dhar SK & Dutta A (2000) Identification and Characterization of the Human ORC6
612 Homolog. *Journal of Biological Chemistry* 275: 34983–34988

613 Duncker BP, Chesnokov IN & McConkey BJ (2009) The origin recognition complex
614 protein family. *Genome Biol* 10: 214

615 Gemble S, Wardenaar R, Keuper K, Srivastava N, Nano M, Macé A-S, Tijhuis AE,
616 Bernhard SV, Spierings DCJ, Simon A, *et al* (2022) Genetic instability from a
617 single S phase after whole-genome duplication. *Nature* 604: 146–151

618 Hayashi-Takanaka Y, Hayashi Y, Hirano Y, Miyawaki-Kuwakado A, Ohkawa Y, Obuse
619 C, Kimura H, Haraguchi T & Hiraoka Y (2021) Chromatin loading of MCM
620 hexamers is associated with di-/tri-methylation of histone H4K20 toward
621 S phase entry. *Nucleic Acids Res* 49: 12152–12166

622 Hayashi-Takanaka Y, Kina Y, Nakamura F, Becking LE, Nakao Y, Nagase T, Nozaki N
623 & Kimura H (2020) Histone modification dynamics as revealed by multicolor
624 immunofluorescence-based single-cell analysis. *J Cell Sci* 133: jcs243444

625 Hayashi-Takanaka Y, Maehara K, Harada A, Umehara T, Yokoyama S, Obuse C,
626 Ohkawa Y, Nozaki N & Kimura H (2015) Distribution of histone H4
627 modifications as revealed by a panel of specific monoclonal antibodies.
628 *Chromosome Res* 23: 753–766

629 Hayashi-Takanaka Y, Yamagata K, Nozaki N & Kimura H (2009) Visualizing histone
630 modifications in living cells: spatiotemporal dynamics of H3 phosphorylation
631 during interphase. *J Cell Biol* 187: 781–790

632 Hayashi-Takanaka Y, Yamagata K, Wakayama T, Stasevich TJ, Kainuma T, Tsurimoto
633 T, Tachibana M, Shinkai Y, Kurumizaka H, Nozaki N, *et al* (2011) Tracking

epigenetic histone modifications in single cells using Fab-based live endogenous modification labeling. *Nucleic Acids Research* 39: 6475–6488

Hu Y & Stillman B (2023) Origins of DNA replication in eukaryotes. *Mol Cell* 83: 352–372

Huang W, Hickson LJ, Eirin A, Kirkland JL & Lerman LO (2022) Cellular senescence: the good, the bad and the unknown. *Nat Rev Nephrol* 18: 611–627

Ishimi Y (2018) Regulation of MCM2-7 function. *Genes Genet Syst* 93: 125–133

Johmura Y, Shimada M, Misaki T, Naiki-Ito A, Miyoshi H, Motoyama N, Ohtani N, Hara E, Nakamura M, Morita A, *et al* (2014) Necessary and Sufficient Role for a Mitosis Skip in Senescence Induction. *Molecular Cell* 55: 73–84

Kinyamu HK, Bennett BD, Bushel PR & Archer TK (2020) Proteasome inhibition creates a chromatin landscape favorable to RNA Pol II processivity. *J Biol Chem* 295: 1271–1287

Li C-J & DePamphilis ML (2002) Mammalian Orc1 Protein Is Selectively Released from Chromatin and Ubiquitinated during the S-to-M Transition in the Cell Division Cycle. *Molecular and Cellular Biology* 22: 105–116

Limas JC & Cook JG (2019) Preparation for DNA replication: the key to a successful S phase. *FEBS Lett* 593: 2853–2867

Lin Y-C, Liu D, Chakraborty A, Kadyrova LY, Song YJ, Hao Q, Mitra J, Hsu RYC, Arif MK, Adusumilli S, *et al* (2022) Orc6 is a component of the replication fork and enables efficient mismatch repair. *Proc Natl Acad Sci U S A* 119: e2121406119

Lin Y-C, Liu D, Chakraborty A, Macias V, Brister E, Sonalkar J, Shen L, Mitra J, Ha T, Kajdacsy-Balla A, *et al* (2023) DNA Damage-Induced, S-Phase Specific Phosphorylation of Orc6 is Critical for the Maintenance of Genome Stability. *Mol Cell Biol* 43: 143–156

López S, Lim EL, Horswell S, Haase K, Huebner A, Dietzen M, Mourikis TP, Watkins TBK, Rowan A, Dewhurst SM, *et al* (2020) Interplay between whole-genome doubling and the accumulation of deleterious alterations in cancer evolution. *Nat Genet* 52: 283–293

Makino Y, Yogosawa S, Kanemaki M, Yoshida T, Yamano K, Kishimoto T, Moncollin V, Egly JM, Muramatsu M & Tamura T (1996) Structures of the rat proteasomal ATPases: determination of highly conserved structural motifs and rules for their spacing. *Biochem Biophys Res Commun* 220: 1049–1054

Makino Y, Yoshida T, Yogosawa S, Tanaka K, Muramatsu M & Tamura TA (1999) Multiple mammalian proteasomal ATPases, but not proteasome itself, are associated with TATA-binding protein and a novel transcriptional activator, TIP120. *Genes Cells* 4: 529–539

Méndez J, Zou-Yang XH, Kim S-Y, Hidaka M, Tansey WP & Stillman B (2002) Human Origin Recognition Complex Large Subunit Is Degraded by Ubiquitin-Mediated Proteolysis after Initiation of DNA Replication. *Molecular Cell* 9: 481–491

Nishitani H, Sugimoto N, Roukos V, Nakanishi Y, Saijo M, Obuse C, Tsurimoto T, Nakayama KI, Nakayama K, Fujita M, *et al* (2006) Two E3 ubiquitin ligases, SCF-Skp2 and DDB1-Cul4, target human Cdt1 for proteolysis. *EMBO J* 25: 1126–1136

Nozawa R-S, Nagao K, Masuda H-T, Iwasaki O, Hirota T, Nozaki N, Kimura H & Obuse C (2010) Human POGZ modulates dissociation of HP1alpha from mitotic chromosome arms through Aurora B activation. *Nat Cell Biol* 12: 719–727

Ogawa Y, Takahashi T & Masukata H (1999) Association of fission yeast Orp1 and Mcm6 proteins with chromosomal replication origins. *Mol Cell Biol* 19: 7228–7236

Okano-Uchida T, Kent LN, Ouseph MM, McCarty B, Frank JJ, Kladney R, Cuitino MC, Thompson JC, Coppola V, Asano M, *et al* (2018) Endoreduplication of the mouse genome in the absence of ORC1. *Genes Dev* 32: 978–990

Ortega MA, Nguyen H & Ward WS (2016) ORC proteins in the mammalian zygote. *Cell Tissue Res* 363: 195–200

Pan Q, Li F, Ding Y, Huang H & Guo J (2022) ORC6 acts as a biomarker and reflects poor outcome in clear cell renal cell carcinoma. *J Cancer* 13: 2504–2514

Panopoulos A, Pacios-Bras C, Choi J, Yenjerla M, Sussman MA, Fotedar R & Margolis RL (2014) Failure of cell cleavage induces senescence in tetraploid primary cells.

Mol Biol Cell 25: 3105–3118

Prasanth SG, Prasanth KV & Stillman B (2002) Orc6 Involved in DNA Replication, Chromosome Segregation, and Cytokinesis. *Science* 297: 1026–1031

Quan Y, Xia Y, Liu L, Cui J, Li Z, Cao Q, Chen XS, Campbell JL & Lou H (2015) Cell-Cycle-Regulated Interaction between Mcm10 and Double Hexameric Mcm2-7 Is Required for Helicase Splitting and Activation during S Phase. *Cell Reports* 13: 2576–2586

Sabath N, Levy-Adam F, Younis A, Rozales K, Meller A, Hadar S, Soueid-Baumgarten S & Shalgi R (2020) Cellular proteostasis decline in human senescence. *Proc Natl Acad Sci U S A* 117: 31902–31913

Samson RY, Abeyrathne PD & Bell SD (2016) Mechanism of Archaeal MCM Helicase Recruitment to DNA Replication Origins. *Mol Cell* 61: 287–296

Semple JW, Da-Silva LF, Jervis EJ, Ah-Kee J, Al-Attar H, Kummer L, Heikkila JJ, Pasero P & Duncker BP (2006) An essential role for Orc6 in DNA replication through maintenance of pre-replicative complexes. *EMBO J* 25: 5150–5158

Sheu Y-J & Stillman B (2006) Cdc7-Dbf4 Phosphorylates MCM Proteins via a Docking Site-Mediated Mechanism to Promote S Phase Progression. *Molecular Cell* 24: 101–113

Shi K, Zhang J-Z, Zhao R-L, Yang L & Guo D (2018) PSMD7 downregulation induces apoptosis and suppresses tumorigenesis of esophageal squamous cell carcinoma via the mTOR/p70S6K pathway. *FEBS Open Bio* 8: 533–543

Sugimoto N, Maehara K, Yoshida K, Ohkawa Y & Fujita M (2018) Genome-wide analysis of the spatiotemporal regulation of firing and dormant replication origins in human cells. *Nucleic Acids Res* 46: 6683–6696

Tang M, Chen J, Zeng T, Ye D-M, Li Y-K, Zou J & Zhang Y-P (2023) Systemic analysis of the DNA replication regulator origin recognition complex in lung adenocarcinomas identifies prognostic and expression significance. *Cancer Med* 12: 5035–5054

Tatsumi Y, Ohta S, Kimura H, Tsurimoto T & Obuse C (2003) The ORC1 Cycle in Human Cells. *Journal of Biological Chemistry* 278: 41528–41534

Thakur BL, Ray A, Redon CE & Aladjem MI (2022) Preventing excess replication origin activation to ensure genome stability. *Trends Genet* 38: 169–181

Torres C, Lewis L & Cristofalo VJ (2006) Proteasome inhibitors shorten replicative life span and induce a senescent-like phenotype of human fibroblasts. *J Cell Physiol* 207: 845–853

Ukekawa R, Maegawa N, Mizutani E, Fujii M & Ayusawa D (2004) Proteasome inhibitors induce changes in chromatin structure characteristic of senescent human fibroblasts. *Biosci Biotechnol Biochem* 68: 2395–2397

Vashee S, Simancek P, Challberg MD & Kelly TJ (2001) Assembly of the human origin recognition complex. *J Biol Chem* 276: 26666–26673

Vassilev A & DePamphilis M (2017) Links between DNA Replication, Stem Cells and Cancer. *Genes* 8: 45

Vilchez D, Saez I & Dillin A (2014) The role of protein clearance mechanisms in organismal ageing and age-related diseases. *Nat Commun* 5: 5659

Walter D, Hoffmann S, Komseli E-S, Rappsilber J, Gorgoulis V & Sørensen CS (2016) SCFCyclin F-dependent degradation of CDC6 suppresses DNA re-replication. *Nat Commun* 7: 10530

Xu N, You Y, Liu C, Balasov M, Lun LT, Geng Y, Fung CP, Miao H, Tian H, Choy TT, *et al* (2020) Structural basis of DNA replication origin recognition by human Orc6 protein binding with DNA. *Nucleic Acids Research* 48: 11146–11161

Zeng J, Hills SA, Ozono E & Diffley JFX (2023) Cyclin E-induced replicative stress drives p53-dependent whole-genome duplication. *Cell* 186: 528-542.e14

Zhou Y, Pozo PN, Oh S, Stone HM & Cook JG (2020) Distinct and sequential re-replication barriers ensure precise genome duplication. *PLoS Genet* 16: e1008988

Figure Legends

Figure 1. Detection of chromatin-bound Orc6 by single-cell plot analysis

(**A**) Representative fluorescence images of Hoechst, EdU, Orc6, and Orc2 in hTERT-RPE1 cells prepared using the direct fixation method (upper panels) and the pre-extraction method (lower panels). Scale bars, 10 µm. (**B**) Single-cell plot analysis based on the images in (**A**). Each dot represents the intensities of EdU, Orc6, and Orc2 in a single individual cell against the Hoechst intensities. The orange dots represent S-phase cells based on EdU intensities ($\log_2$[EdU] >−2). n = 450 (number of cells examined in each panel).

Figure 2. Effects of proteasome inhibitors on the dynamics of Orc6 during the cell cycle

(**A**) Single-cell plot analysis of Orc6 (top), Cdt1 (middle), and Orc2 (bottom) in hTERT-RPE1 cells. Cells were treated with 20 µM MG132 for 0, 1, 2, or 4 h (timescale on the top), fixed using the direct fixation method (left panels) and the pre-extraction method (right panels), and stained simultaneously with anti-Orc6, anti-Cdt1, and anti-Orc2 antibodies. The cells were counterstained with Hoechst. Each dot represents the intensity of Orc6, Cdt1, and Orc2 in a single individual cell plotted against the Hoechst intensity. n = 450 (number of cells examined in each panel). (**B**) Orc6, Cdt1, and Orc2 levels in the S-phase cells. Cells corresponding to the S phase (1.1< Hoechst <1.75) are selected from (**A**), and their fluorescence intensities were plotted. The average intensity in MG132-untreated cells was defined as 1. (**C**) Schematic diagram of the biochemical fractionation method for whole-cell lysates and chromatin fractions. (**D**) Western blotting analysis using antibodies against Orc6, Cdt1, Orc2, histone H3, and GAPDH. hTERT-RPE1 cells were treated with 20 µM MG132 for the indicated time periods (h). Whole-cell lysates (left) and chromatin fractions (right) were prepared as described above and analyzed using western blotting. Histone H3 and GAPDH are loading controls. The positions of molecular mass markers (kDa) are indicated to the right.

Figure 3. Aberrantly high levels of chromatin-bound Orc6 and Mcm2 in aged fibroblast cells

(**A**) IMR90 cells (passage numbers 18 and 32) were fixed using the pre-extraction method and stained using Hoechst, anti-Orc6, and anti-Mcm2 antibodies.

Representative fluorescence images are shown. Arrows indicate the relatively larger nucleus with high Orc6 signals. Scale bars, 10 µm. (**B**) Single-cell plot analysis based on the images in (**A**). Each dot represents the intensities of Orc6 and Mcm2 in an individual cell plotted against the Hoechst intensities. The magenta dots in the Orc6 panels represent cells with fluorescent signals of Hoechst >1.8 and $\log_2$(Orc6) >0.5. The same cells were marked by magenta in the Mcm2 panels. The red-boxed regions represent cells with high MCM levels ($\log_2$[Mcm2] >−1) and high DNA content (Hoechst >1.8), and the blue-boxed regions represent cells with low MCM levels ($\log_2$[Mcm2] <−1) and high DNA content (Hoechst >1.8). n = 450 (number of cells examined in each panel).

Figure 4. Inhibition of proteasome activity causes cellular senescence and aberrantly high levels of chromatin-bound Orc6 and MCM

(**A**) Representative fluorescence images of Hoechst and p21 staining in hTERT-RPE1 cells treated with DMSO or 312 nM MG132 for 18 h. Cells were fixed using the direct fixation method. Scale bars, 10 µm. (**B**) Western blotting analysis of whole-cell lysates using antibodies against p21 and GAPDH. hTERT-RPE1 cells were treated with DMSO as a control or 312 nM MG132 for 1 day before harvesting. The positions of molecular mass markers (kDa) are indicated to the right. GAPDH is a loading control. (**C**) Single-cell plot analysis of Orc6 (top), Mcm3 (middle), and Cdt1 (bottom) in hTERT-RPE1 cells. Cells were treated with DMSO as a control or the indicated concentrations of MG132 for 18 h, fixed using the pre-extraction method, and stained with Hoechst, anti-Orc6, anti-Mcm3, and anti-Cdt1 antibodies. The cells showing high Orc6 levels ($\log_2$[Orc6] >0.5) and high DNA content (Hoechst >1.8) are marked magenta in the Orc6 panels. The same cells are marked magenta also in the Mcm3 and Cdt1 panels. n = 450 (cells examined in each panel). The red-boxed regions represent cells with high Mcm3 levels and high DNA content, and the blue-boxed region represents cells with low Mcm3 levels and high DNA content. (**D**) Single-cell plot analysis of Mcm2 (top) and histone H3S10ph (bottom) in hTERT-RPE1 cells. Cells were treated with DMSO as a control or 312 nM MG132 for the indicated time periods. n = 450 (number of cells examined in each panel). The cells showing high H3S10ph levels ($\log_2$[H3S10ph] >1) are marked magenta in the H3S10ph panels. The blue-circled regions represent cells with low Mcm2 levels and high DNA content. The red-boxed regions represent cells with high Mcm2 and high DNA content. (**E**) Efficiency of siRNA knockdown of PSMD7 expression. hTERT-RPE1 cells were treated with siRNA for the negative control or PSMD7 for 2 days before harvesting. Western blotting analysis of

whole-cell lysates was performed using antibodies against PSMD7 and GAPDH. The positions of molecular mass markers (kDa) are indicated to the right. GAPDH is a loading control. (**F**) Single-cell plot analysis of Orc6 and Mcm2 in hTERT-RPE1 cells treated with negative control-siRNA (siControl) or PSMD7-siRNA (siPSMD7). Cells were treated with the indicated siRNA for 2 days, fixed using the pre-extraction method, and stained with Hoechst, anti-Orc6, and anti-Mcm2 antibodies. The cells showing high Orc6 levels ($\log_2$[Orc6] >0.5) and high DNA content (Hoechst >1.8) are marked magenta in the Orc6 panels. The same cells are marked magenta also in the Mcm2 panels. The red-boxed region represents cells with high Mcm2 levels ($\log_2$[Mcm2] >−2) and high DNA content (Hoechst >1.8), and the blue-boxed region represents cells with low Mcm2 levels ($\log_2$[Mcm2] <−2) and high DNA content (Hoechst >1.8). n = 500 (number of cells examined in each panel).

Figure 5. Detection of cell cycle progression in tetraploid cells and Orc6 behavior

(**A**) Timing diagram of MG132 treatment and EdU labeling used in (**B**). hTERT-RPE1 cells were incubated with 312 nM MG132 for a day (day 1) (left panels in **B**), washed with fresh medium without MG132, and incubated for another day (day 2) (right panels in **B**). The cells were labeled with EdU for 30 min before the sample collection on day 1 and day 2. (**B**) Single-cell plot analysis of EdU (top), Mcm2 (middle), and Orc6 (bottom). Cells were fixed using the pre-extraction method and stained with Hoechst, anti-EdU, anti-Mcm2, and anti-Orc6 antibodies. The orange dots represent S-phase cells based on EdU intensities ($\log_2$[EdU] >2). The red-boxed regions represent cells with high Mcm2 levels ($\log_2$[Mcm2] >−1) and high DNA contents (1.8< Hoechst <2.1). n = 600 (cells examined in each panel). (**B'**) The same data from (**B**) is reused, although it was marked differently. The cells showing high Orc6 levels ($\log_2$[Orc6] >0.5) and high DNA content (Hoechst >1.8) are marked magenta in the Orc6 panels. The same cells are marked magenta also in the Mcm2 panels. The red-boxed region represents cells with high Mcm2 levels ($\log_2$[Mcm2] >−0.5) and high DNA content (1.8< Hoechst <2.1), and the blue-boxed region represents cells with low Mcm2 levels ($\log_2$[Mcm2] <0.5) and high DNA content (1.8< Hoechst <2.1). (**C**) Representative fluorescence images of Hoechst, Orc6, and Mcm2 staining used in single cell plot analysis in (**B'**). Red and blue arrows indicated typical cells in the red and blue boxes, respectively, in Figure (**B'**). Scale bars, 10 µm.

Figure 6. Effects of Orc6 depletion on the formation of tetraploid cells

(**A**) Timing diagram of siRNA treatment. Cells were treated with siRNA against a negative control (siControl), Orc1 as a positive control (siOrc1), or Orc6 (siOrc6) for 42 h. (**B**) Western blotting analysis using antibodies against Orc6, Orc1, and histone H3 for the whole-cell fraction from hTERT-RPE1 cells treated with siRNA against a negative control (siControl), Orc1 (siOrc1), and Orc6 (siOrc6). The positions of molecular mass markers (kDa) are indicated to the right. (**C**) Single-cell plot analysis of Mcm2 in hTERT-RPE1 cells treated with siRNA (siControl, siOrc1, or siOrc6). Cells were treated with siRNA, fixed using the pre-extraction method, and stained with Hoechst and anti-Mcm2 antibody. n = 450 (number of cells examined in each panel). (**D**) Timing diagram of siRNA treatment and addition of 312 nM MG132. hTERT-RPE1 cells were treated with siRNA. After 18 h, MG132 was added to the medium at a final concentration of 312 nM, and the cells were incubated for an additional 24 h in the presence of siRNA. (**E**) Single-cell plot analysis of Mcm2 in the cells treated with siRNA (siControl, siOrc1, or siOrc6). Cells showing high Mcm2 levels ($\log_2$[Mcm2] >−1.5) and high DNA content (Hoechst > 1.8) are marked magenta. n = 450 (number of cells examined in each panel). (**F**) Percentages of the magenta-marked cells ($\log_2$[Mcm2] >−1.5 and Hoechst >1.8) among the total G2 phase cells (Hoechst >1.8) calculated based on (**E**). Columns and error bars represent the mean and standard deviation of four independent experimental results. Statistical differences (p = 0.0006) were determined using a one-sided t-test. (**G**) Western blotting analysis using antibodies against Cdc6 and GAPDH for whole-cell lysates from cells treated with siRNA against negative control (siControl) or Cdc6 (siCdc6), as described in (**D**). The positions of molecular mass markers (kDa) are indicated to the right. (**H)** Single-cell plot analysis of chromatin-bound Mcm2 in hTERT-RPE1 cells treated with siRNA (siControl or siCdc6) as described in (**D**). Cells were treated with siRNA against the negative control (siControl) or Cdc6 (siCdc6). After incubation with MG132, the cells were fixed using the pre-extraction method and stained with Hoechst and anti-Mcm2 antibody. Cells showing high MCM levels ($\log_2$[Mcm2] >−2) and high DNA content (Hoechst >1.8) are marked magenta. n = 450 (number of cells examined in each panel).

Figure 8. Schematic diagram of Orc6 behavior

(**A**) Process with normal proteasome activity. After DNA replication, Cdt1 and Orc1 proteins are degraded, and Orc6 is removed from the chromatin, preventing MCM reloading. These cells enter mitosis and produce normal diploid cells. Orc2–5 represents a complex of Orc2, Orc3, Orc4, and Orc5. (**B**) When cells lose proteasome activity,

Orc6, Orc1, Cdt1, and MCM are reloaded onto chromatin, producing tetraploid cells by skipping mitosis.

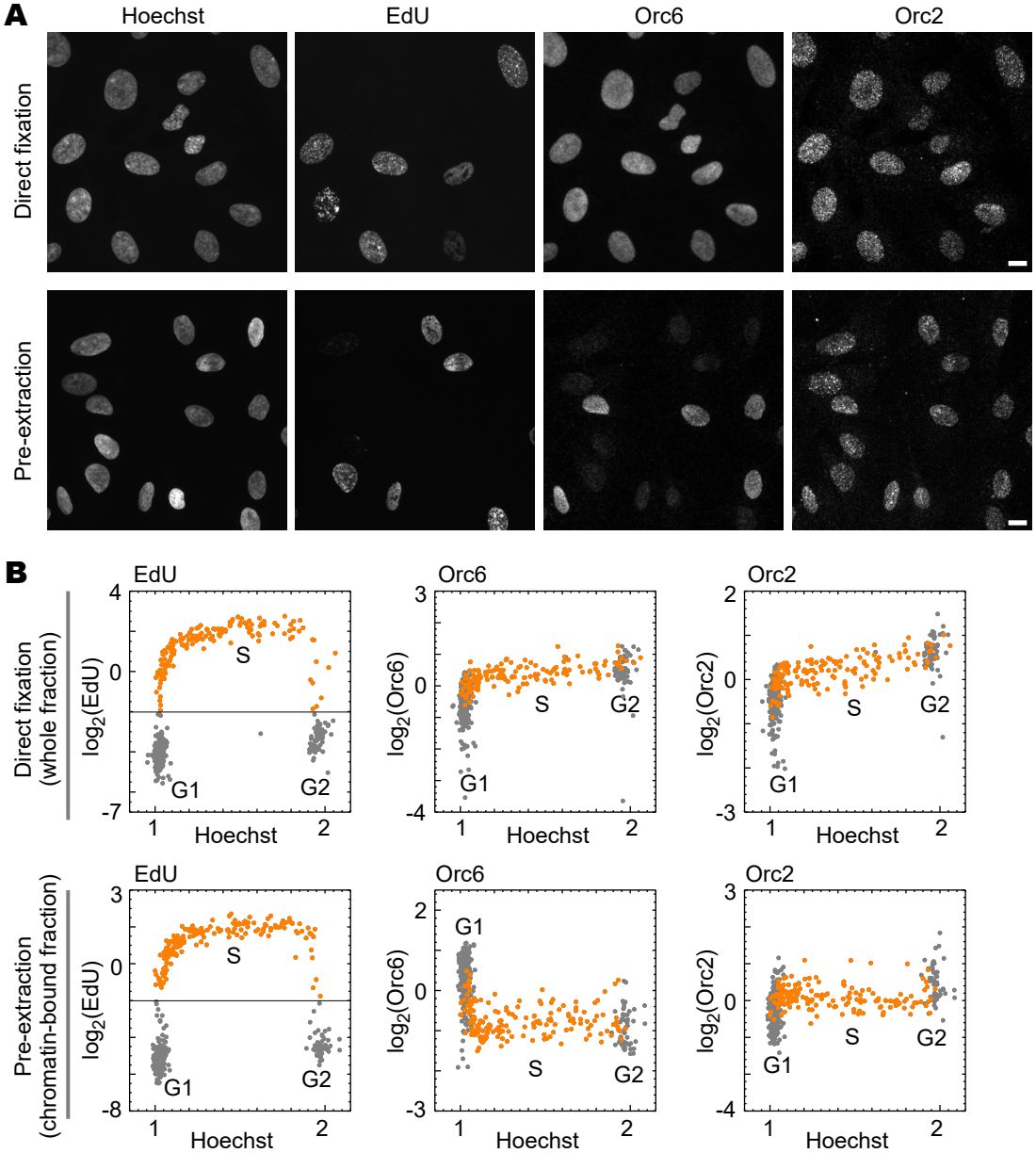
A
Hoechst
EdU
Orc6
Orc2
Direct fixation
Pre-extraction
B
EdU
Orc6
Orc2
Direct fixation
(whole fraction)
Pre-extraction
(chromatin-bound fraction)
log2(EdU)
log2(Orc6)
log2(Orc2)
Hoechst
G1
S
G2

Figure 1

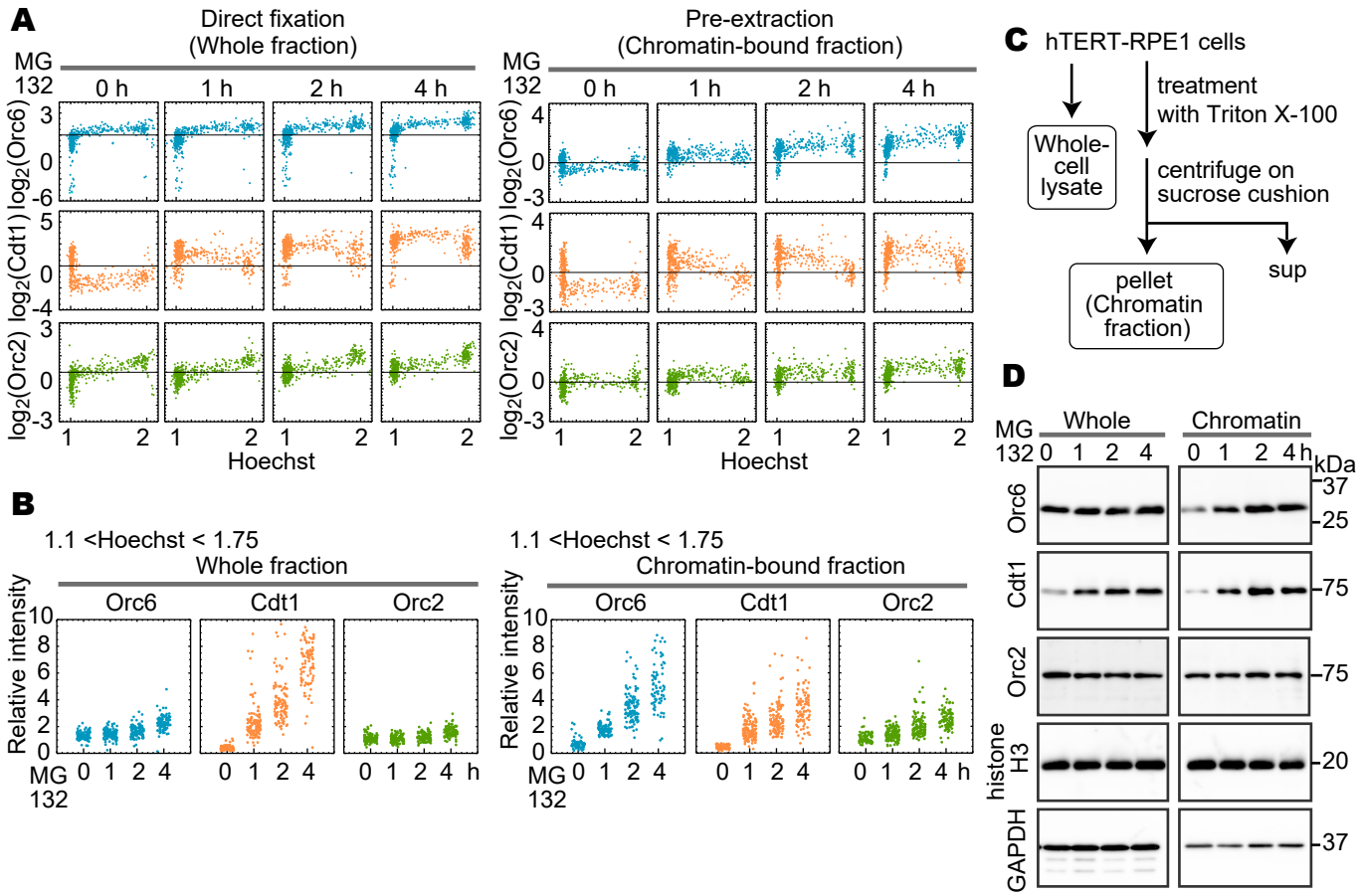
A
Direct fixation
(Whole fraction)
Pre-extraction
(Chromatin-bound fraction)
MG
132
0 h
1 h
2 h
4 h
log2(Orc6)
log2(Cdt1)
log2(Orc2)
Hoechst
B
1.1 <Hoechst < 1.75
Whole fraction
Chromatin-bound fraction
Orc6
Cdt1
Orc2
Relative intensity
C
hTERT-RPE1 cells
treatment
with Triton X-100
Whole-
cell
lysate
centrifuge on
sucrose cushion
pellet
(Chromatin
fraction)
sup
D
Whole
Chromatin
kDa
histone
H3
GAPDH

Figure 2

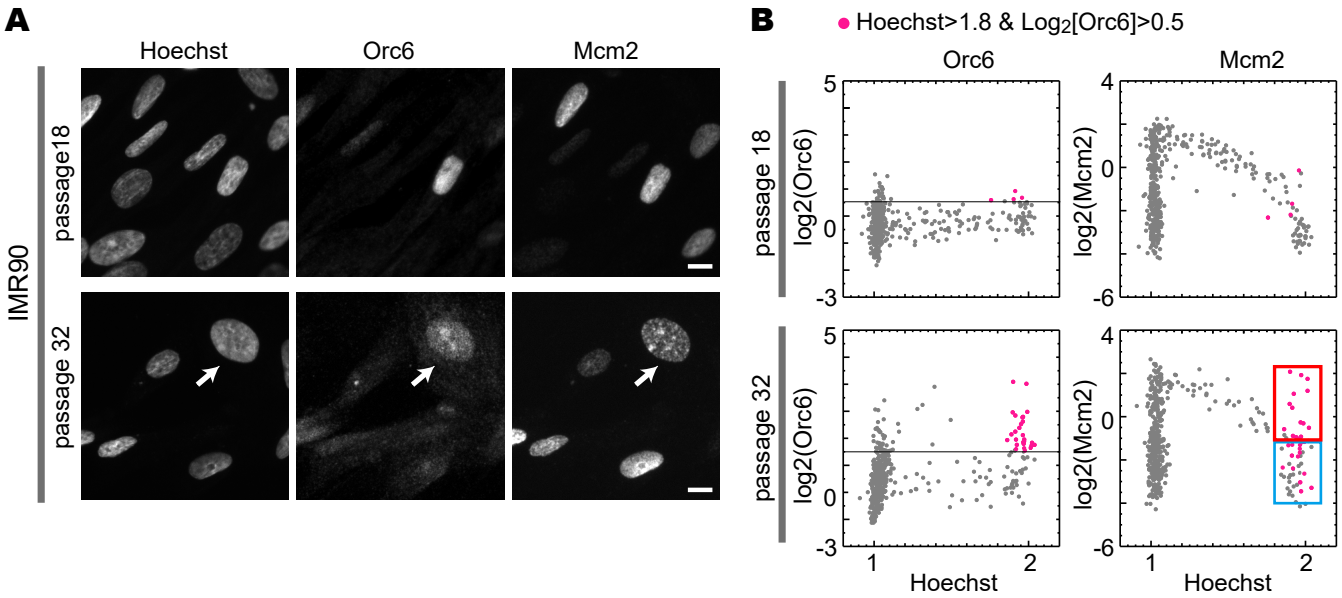
A
Hoechst
Orc6
Mcm2
IMR90
passage18
passage 32
B
Hoechst>1.8 & Log2[Orc6]>0.5
Orc6
Mcm2
passage 18
passage 32
log2(Orc6)
log2(Mcm2)
5
0
-3
4
0
-6
1
2
Hoechst

Figure 3

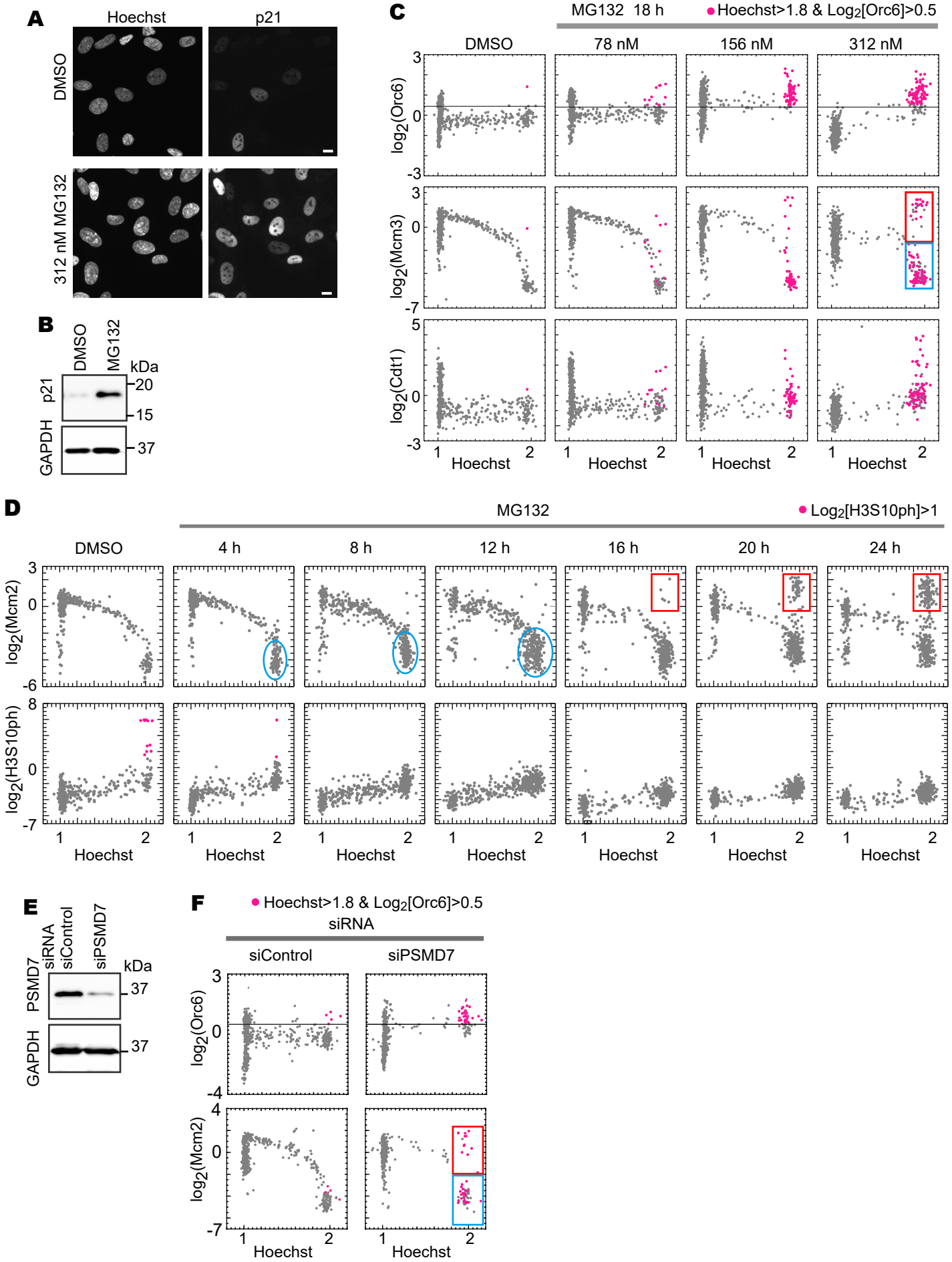
A
Hoechst
p21
DMSO
312 nM MG132
B
DMSO
MG132
kDa
p21
20
15
GAPDH
37
C
MG132 18 h
Hoechst>1.8 & Log2[Orc6]>0.5
DMSO
78 nM
156 nM
312 nM
log2(Orc6)
log2(Mcm3)
log2(Cdt1)
Hoechst
D
MG132
Log2[H3S10ph]>1
DMSO
4 h
8 h
12 h
16 h
20 h
24 h
log2(Mcm2)
log2(H3S10ph)
Hoechst
E
siRNA
siControl
siPSMD7
kDa
PSMD7
37
GAPDH
37
F
Hoechst>1.8 & Log2[Orc6]>0.5
siRNA
siControl
siPSMD7
log2(Orc6)
log2(Mcm2)
Hoechst

Figure 4

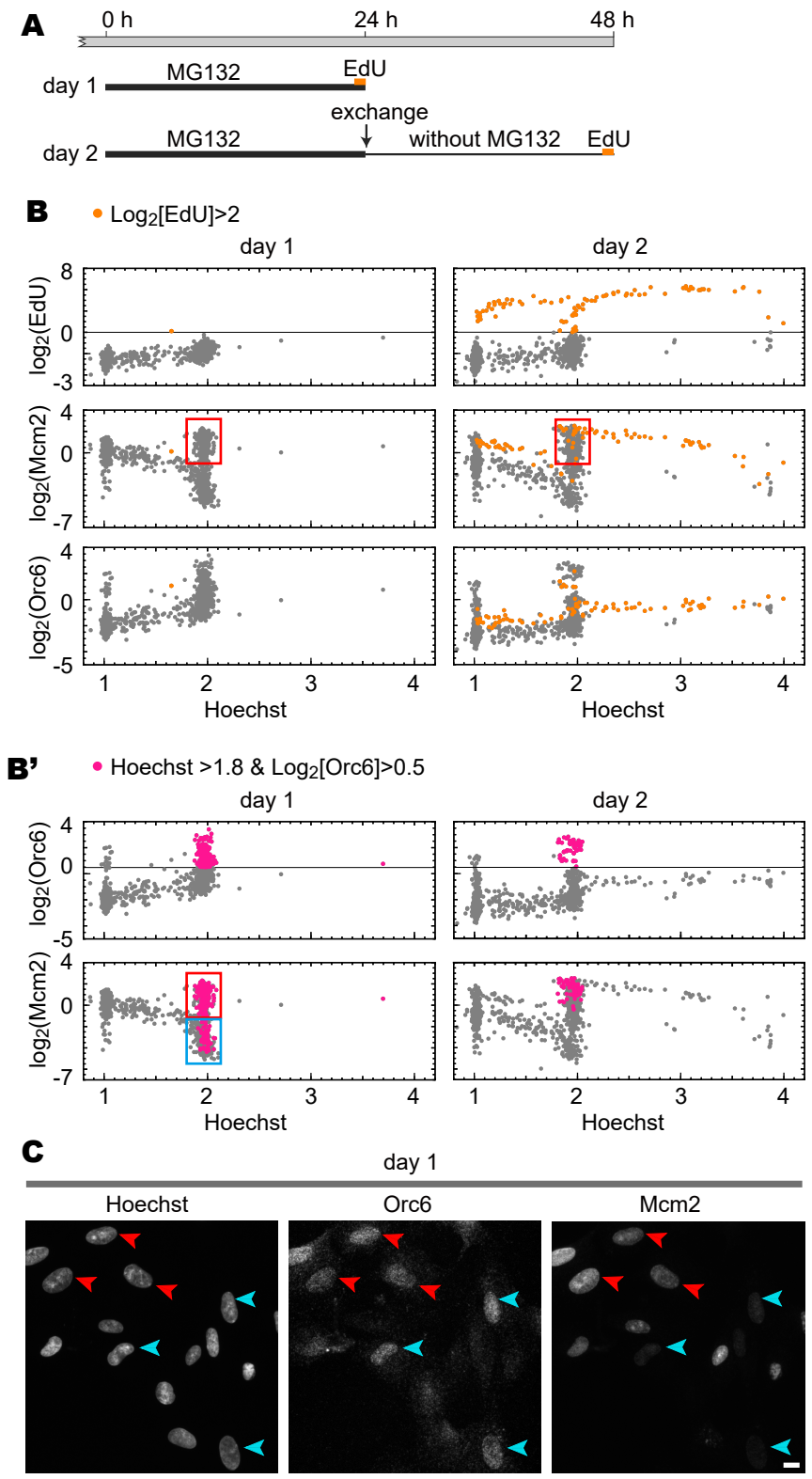
A
0 h
24 h
48 h
day 1
MG132
EdU
exchange
day 2
MG132
without MG132
EdU
B
Log2[EdU]>2
day 1
day 2
log2(EdU)
log2(Mcm2)
log2(Orc6)
Hoechst
B'
Hoechst >1.8 & Log2[Orc6]>0.5
day 1
day 2
log2(Orc6)
log2(Mcm2)
Hoechst
C
day 1
Hoechst
Orc6
Mcm2

Figure 5

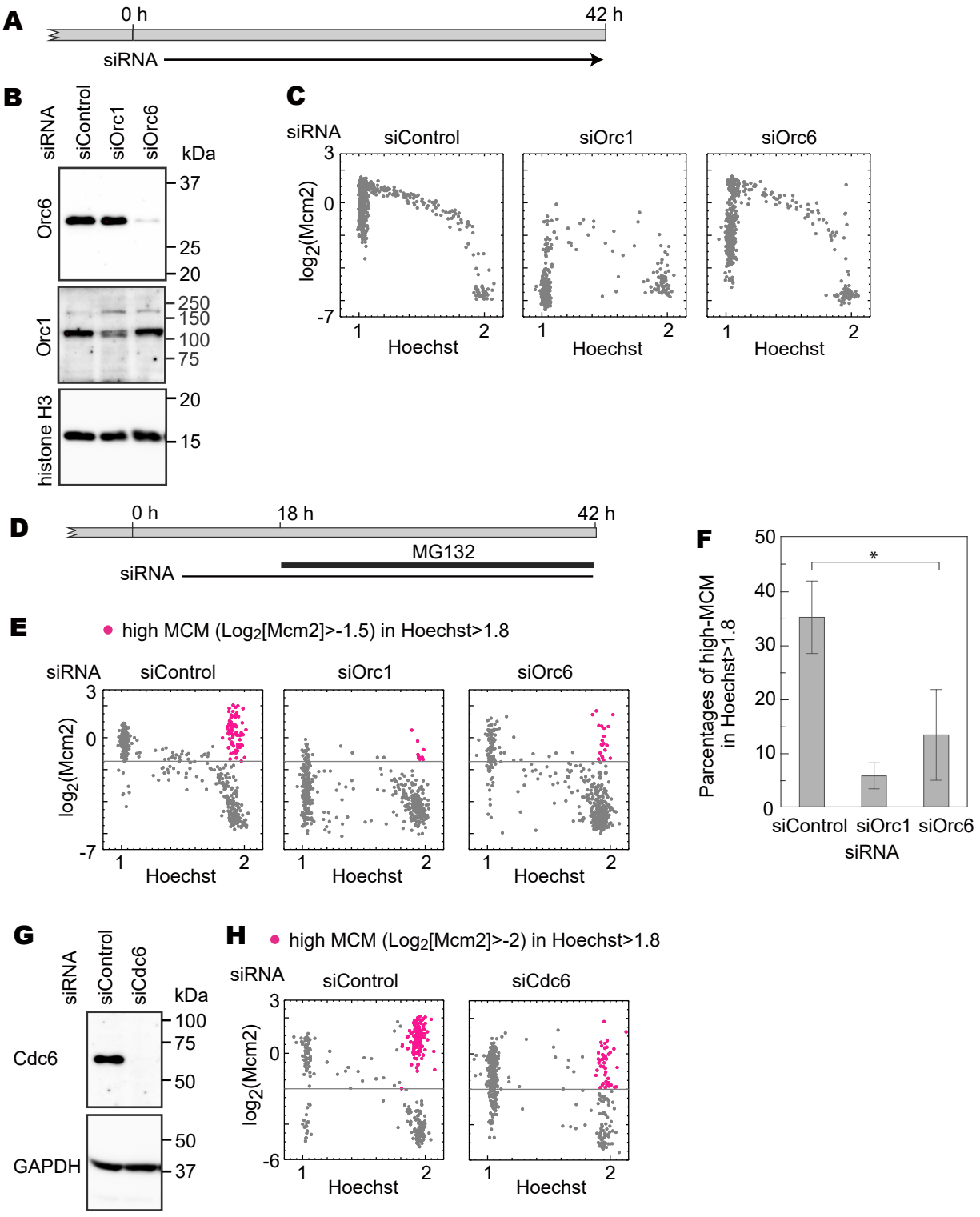
A
0 h
42 h
siRNA
B
siRNA
siControl
siOrc1
siOrc6
kDa
Orc6
37
25
20
Orc1
250
150
100
75
histone H3
20
15
C
siRNA
siControl
siOrc1
siOrc6
log2(Mcm2)
3
0
-7
1
2
Hoechst
D
0 h
18 h
42 h
MG132
siRNA
E
high MCM (Log2[Mcm2]>-1.5) in Hoechst>1.8
siRNA
siControl
siOrc1
siOrc6
log2(Mcm2)
3
0
-7
1
2
Hoechst
F
Parcentages of high-MCM in Hoechst>1.8
50
40
30
20
10
0
*
siControl
siOrc1
siOrc6
siRNA
G
siRNA
siControl
siCdc6
kDa
Cdc6
100
75
50
GAPDH
50
37
H
high MCM (Log2[Mcm2]>-2) in Hoechst>1.8
siRNA
siControl
siCdc6
log2(Mcm2)
3
0
-6
1
2
Hoechst

Figure 6

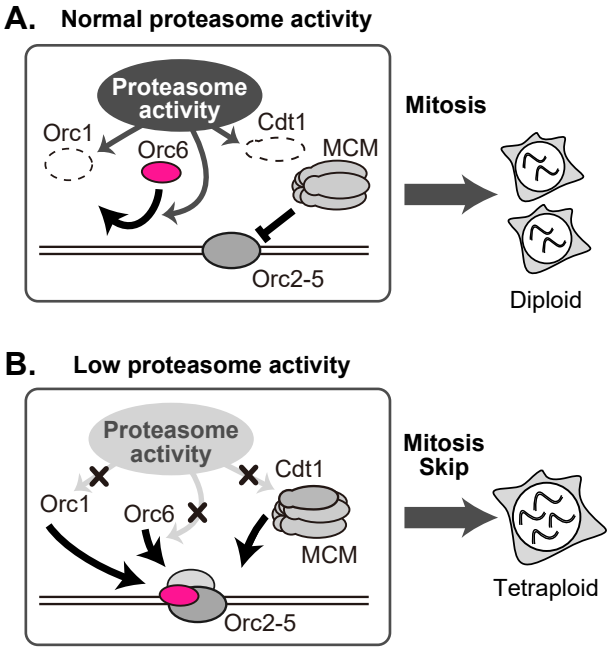
A.
Normal proteasome activity
Proteasome activity
Orc1
Orc6
Cdt1
MCM
Orc2-5
Mitosis
Diploid
B.
Low proteasome activity
Proteasome activity
Orc1
Orc6
Cdt1
MCM
Orc2-5
Mitosis Skip
Tetraploid

Figure 7